Contaminants in Aquatic and Terrestrial Environments

A new in situ method for tracing denitrification in riparian groundwater

Andrea L. Popp, Cara C. Manning, Matthias S. Brennwald, and Rolf Kipfer

Environ. Sci. Technol., **Just Accepted Manuscript** • DOI: 10.1021/acs.est.9b05393 • Publication Date (Web): 06 Jan 2020

A new in situ method for tracing denitrification in riparian groundwater

Andrea L. Popp,[*,†,‡] Cara C. Manning,[¶] Matthias S. Brennwald,[†] and Rolf Kipfer[†,§,‖]

†*Department of Water Resources and Drinking Water, Eawag, 8600 Dübendorf, Switzerland*

[1] ‡*Department of Environmental Systems Science, ETH Zurich, 8000 Zurich, Switzerland*

¶*Department of Earth, Ocean and Atmospheric Sciences, University of British Columbia, V6T 1Z4 Vancouver, Canada*

§*Department of Environmental Systems Science, ETH Zurich, 8092 Zurich, Switzerland*

‖*Isotope Geology, Department of Earth Sciences, ETH Zurich, 8092 Zurich, Switzerland*

E-mail: andrea.popp@eawag.ch

Phone: +41 (0)58 765 5109

Abstract

The spatio-temporal dynamics of denitrification in groundwater are still not well understood due to a lack of efficient methods to quantify this biogeochemical reaction pathway. Previous research used the ratio of N_2 to argon (Ar) to quantify net production of N_2 via denitrification by separating the biologically-generated N_2 component from the atmospheric-generated components. However, this method does not allow to quantify the atmospheric components accurately since the differences in gas partitioning between N_2 and Ar are being neglected. Moreover, conventional (noble) gas analysis in water is both expensive and labor-intensive. We overcome these limitations by using a portable mass spectrometer system, which enables a fast and efficient in situ analysis of dissolved (noble) gases in groundwater. By analyzing a larger set of (noble) gases (N_2, He, Ar and Kr) combined with a physically meaningful excess air model, we quantified N_2 originating from denitrification. Consequently, we were able to study the spatio-temporal dynamics of N_2 production due to denitrification in riparian groundwater over a six-month period. Our results show that denitrification is highly variable in space and time, emphasizing the need for spatially and temporally resolved data to accurately account for denitrification dynamics in groundwater.

Introduction

One of the most prevalent water quality threats in many parts of the world is excess nitrogen, which primarily results from extensive fertilizer application in agriculture.[1–3] Water quality impacts of excess nitrogen are severe and include, but are not limited to, algae blooms and hypoxia, which in turn can have harmful effects on a variety of ecosystems.[3,4]

Excess nitrate (NO_3^-) poses a prevalent and lasting threat to drinking water.[5] Nitrate pollution of the environment is projected to continue rising due to an increasing population, changing land management practices and climate change.[4,6] Thus, it is expected that in future more drinking water sources worldwide will have nitrate concentrations exceeding

potability limits (e.g., the 50 mg/L nitrate threshold of water potability defined by the E.U.[7]).[4,8]

Denitrification is known as the major biogeochemical reaction pathway attenuating nitrate concentrations in water under anoxic conditions.[9–12] This microbially mediated process converts NO_3^- to nitrogen gas (N_2).[13–15] Denitrification depends on (i) the presence of NO_3^-, an electron donor (most commonly—dissolved organic carbon, DOC) and denitrifying bacteria, (ii) the scarcity of O_2 (i.e., anaerobic conditions under which nitrate becomes the microbially preferred electron acceptor instead of O_2), and (iii) favorable ambient conditions regarding temperature and pH (optimum values lie between 25°C and 35°C, and 5.5 and 8.0, respectively).[11] However, the availability of an electron donor and anaerobic conditions are the most critical factors for denitrification.[11]

Well-recognized hotspots for high nitrate removal are riparian zones, which are the dynamic interfaces between streams and shallow groundwater where surface water and groundwater exchange.[16–19] Riparian zones deliver a multitude of ecosystem services by retaining and removing pollutants such as nitrate.[20] In river-aquifer systems, the conditions favorable for denitrification are controlled by the ambient sediment texture (i.e., hydraulic conductivity) and the hydraulic connection between the stream and the surrounding aquifer.[21–23]

Numerous studies have investigated denitrification in (riparian) aquifers at different spatial and temporal scales using a variety of methods.[11,24,25] However, despite the importance of denitrification and technological advancements, the spatio-temporal dynamics of this process remain poorly understood. This is because most conventional methods require discrete sample collection and lab-based analyses—thus most methods available are prohibitively costly and labor-intensive.[10,14,26,27] Ignoring the dynamics of denitrification, however, may lead to insufficient groundwater monitoring for nitrate contamination and an erroneous assessment of water quality.

Previous research[10,14,26] stresses that the fundamental problem regarding studying denitrification is the difficulty of quantifying the end-product, N_2, due to its high atmospheric

background (78% N_2 in air),[28] which makes denitrification "a miserable process to measure".[14]

The atmospheric N_2 component dissolved in groundwater originates from air-water exchange during groundwater recharge which involves gas equilibrium partitioning as well as the ubiquitously observed (partial) dissolution of entrapped air bubbles leading to the formation of excess air (i.e., a surplus of atmospheric gases relative to the atmospheric solubility equilibrium).[29] Dissolved atmospheric, noble gases in groundwater are solely affected by physical processes (i.e., groundwater recharge temperature and excess air), whereas reactive gases such as N_2 are not only affected by physical but also by biogeochemical processes (e.g., denitrification).[30] Therefore, to quantify N_2 stemming from denitrification in groundwater, one needs to separate the different N_2 components: N_2 resulting from air-water gas exchange during groundwater recharge can be identified and quantified using noble gas measurements to model the physical gas partitioning of N_2. Subsequently, N_2 in excess of the atmospheric components can be attributed to denitrification.[31,32]

Previous studies[30–42] have used a combined analysis of N_2 and the noble gas Ar (i.e., the N_2/Ar method) to account for the atmospheric N_2 component and thereby quantify net denitrification in groundwater. Inherently, this approach assumes that air bubbles dissolve completely during excess air formation. This assumption, however, is physically-incorrect since the hydrostatic pressure necessary for the complete dissolution of entrapped air bubbles is almost never sufficient in natural groundwater systems.[43,44] The current scientific consensus on excess air research is that an initially trapped air bubble dissolves only partly, which leads to the formation of excess air that is elementally fractionated (i.e., the water phase is enriched in the heavier, more soluble noble gases with respect to completely dissolved air).[43,44] Therefore, to accurately estimate the atmospheric N_2 components, one needs to quantify i) excess air formation, which is typically fractionated relative to air[43,45–47] and ii) the water recharge temperature which determines the gas solubility equilibrium concentration. The amount and fractionation of excess air, however, can only reliably be estimated if

the concentrations of several noble gas species are available.[43,46,48–50]

Here, we present a new method to overcome the limitations of conventional (noble) gas analysis (i.e., costly and time-consuming) and the commonly used N_2/Ar method (i.e., neglecting excess air fractionation). We employed a recently developed Gas Equilibrium-Membrane Inlet Mass Spectrometer (GE-MIMS) system[51] to obtain spatially and temporally resolved time series data of dissolved gas concentrations including N_2, O_2 as well as the noble gases Ar, helium (He) and krypton (Kr) in groundwater.

Thereby, we were able to quasi-continuously analyze dissolved gas concentrations directly in the field at three different piezometers located in the riparian zone from January until June 2018. Having the concentrations of three different noble gas species available allowed us to estimate the groundwater recharge temperature as well as the amount and fractionation of excess air. Thereby, we can reliably determine the atmospheric N_2 components using in situ noble gas analysis. With the obtained data-set, we consequently explored the spatio-temporal dynamics of denitrification in groundwater over a six-month period.

Gas analysis was complemented by the analyses of DOC and NO_3^- concentrations, which are key factors for denitrification. Moreover, we observed typical transformation products originating from the conversion of NO_3^- to N_2, which include elevated alkalinity and sulfate ion (SO_4^{2-}) concentrations (requiring electron donors like organic matter and pyrite, respectively).[11,52,53] To determine drivers of spatial variability in denitrification, we also determined the local sediment properties as well as the biological activity. All these chemical and sedimentological parameters govern the ambient conditions for denitrification because the hydraulic conductivity of the porous media and the microbial activity control gas and solute transport and can thereby affect denitrification.[22]

The key objectives of this study are to use continuous, on-site (noble) gas spectrometry combined with an excess air model to (i) quantify N_2 stemming from denitrification and to (ii) identify spatio-temporal denitrification dynamics and its drivers in riparian groundwater.

Materials and Methods

Site Description

Our study site is located in northern Switzerland in the city of Dübendorf (Fig. 1). We conducted our experiments at a restored stream reach of the Chriesbach—a heavily urbanized, losing stream.[54] The majority of its length has been channelized and treated wastewater accounts for up to ~30% of the discharge.[55]

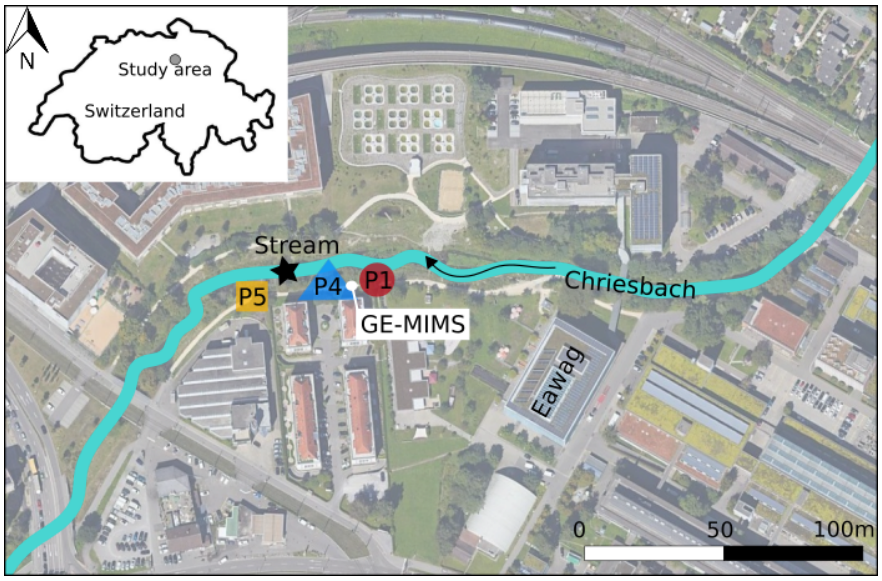

Figure 1: Study area showing the approximate locations of the three piezometers (P1 in red, P4 in blue and P5 in orange) as well as the stream sampling location (in black), the installed GE-MIMS and the surrounding urban area.

The streambed consists of fine sands and loam[54] and is known to be partially clogged due to the settling suspended matter originating from an upstream wastewater treatment plant.[56]

Water from three piezometers (P1, P4 and P5) was weekly (microbiology, water chemistry) and quasi-continuously (gas measurements) analyzed from January until June 2018. The piezometers are located approximately 0.5 m from the stream alongside the streambank (Figs. 1 and S3). Each piezometer is 6 m deep and screened over its entire length. Please note that the groundwater studied represents recently infiltrated river water (that is bank

filtrate) and therefore any reference to groundwater throughout the text relates to shallow groundwater of a riparian aquifer. For more information about aquifer properties, please see Text S2.

Estimating the Hydraulic Conductivity of the Streambank

Stream-aquifer interactions are controlled by hydraulic head gradients and the hydraulic conductivity of the sediments (k).[21,22] The latter defines how easily a fluid flows through a porous matrix and is determined by the sediment texture (such as grain size distribution and packing).[57] To gain insight into the local sediment texture of the streambank at our study site, we conducted slug tests at all piezometers (P1, P4 and P5). Thereby, we estimated the local hydraulic conductivity of the streambank using the Bower-Rice slug test solution.[58]

Analysis of Total Cell Concentrations

The sediment texture governs not only the hydraulic conductivity but also the available area for microbial colonization, thereby impacting the abundance of microbial communities.[59] Microbes can, in turn, alter the hydraulic conductivity through biofilm growth fostering clogging and affecting water residence times and pollutant turnover.[20]

Total cell concentrations (TCC) in water were determined as a rough indicator of denitrification potential in all three piezometers and in the stream using flow cytometry.[60] We sampled TCC as water samples (n=13 at each location from January until June 2018) in 12 ml flasks, which contained para-formaldehyde to fix the microbes. The flasks were cooled immediately after sampling and analyzed the next day at Eawag (see Table S1 for more information).

Analysis of Key Parameters associated with Denitrification

Nitrate, DOC and low oxygen concentrations are essential prerequisites for denitrification to occur, whereas the formation of sulfate and bicarbonate ions (i.e., alkalinity) are typical transformation products associated with denitrification.[11,52,53]

On a weekly basis we sampled these key parameters at all three piezometers and at the stream (except for O_2 concentrations, which were determined continuously; see next section).

For the determination of NO_3^-, DOC, alkalinity and SO_4^{2-} concentrations we took water samples in 1 L Schott glass bottles, which were stored in a cooling room immediately after sampling. The samples were analyzed the following day at Eawag (see Table S1 for instruments used, limits of quantification and uncertainties). For water sampling of the piezometers we used fixed installed groundwater pumps (see next section), except for the streamwater, which was sampled manually.

Continuous Dissolved (Noble) Gas Analysis

For the continuous dissolved (noble) gas analysis we permanently installed a GE-MIMS system[51] in a wooden box with access to a power supply at the study site (Figs. 1 and S3). Three submersible pumps (Comet ECO-PLUS_20000; placed ~3 m below the groundwater table) continuously abstracted groundwater (~0.8 L/min) from the three piezometers. To prevent algae growth and atmospheric gas contamination, we used nontransparent, gas impermeable nitrile tubing for water transport from the wells to the GE-MIMS. The tubing was buried about 30 cm below ground to avoid any extreme cooling or heating of the water. The pumped water was first filtered (Nussbaum, chrome-steel, 10 microns) before flowing to commercially available membrane modules (MiniModule 1x5.5[61]). While water was flowing through the membrane module, a gas equilibrium was established between the gas species dissolved in the sampling water and the gas species in the head space of the module. Through a capillary connecting the head space of the module with the GE-MIMS, a small gas fraction entered the MS for gas analysis.[51] After passing the membrane module,

the water was disposed of into the stream downstream of our study area. Each piezometer had its own water filter and membrane module to allow for quasi-continuous gas analysis.

The GE-MIMS features six different gas inlet ports, which allow for quasi-continuous, consecutive sampling of up to six different sampling locations (although one gas inlet port is usually reserved for the calibration of the MS with ambient air). We used four ports in total: one for each piezometer and one for sampling of ambient air. At every piezometer He, Ar, Kr, N_2 and O_2 were alternately analyzed, which took about 8 minutes for each analysis block, plus two minutes of purging for the gas inlet system between switching inlet ports. After repeating the set of water samples twice, one standard was analyzed. By obtaining a standard approximately every 1.5 hours, we were able to correct for instrument sensitivity drifts, e.g., due to air temperature changes.

Water samples were calibrated by comparing peak heights between ambient air and the gases equilibrated in the head space of the membrane module. Thereby, we could calculate the partial pressures of the respective gas species observed. The partial pressures were converted to dissolved gas concentrations according to the gas-specific Henry coefficients at the respective water temperature (recorded with a MAXIM type DS18B20 sensor placed at the membrane module).

For more details on dissolved (noble) gas theory in riparian aquifers, see Text S1. For more technical details regarding the GE-MIMS system, we refer to Brennwald et al.[51]

Estimating N_2 Production due to Denitrification

The total dissolved N_2 (from here on referred to as $N_{2(tot)}$) consists of atmospheric N_2 components and N_2 originating from denitrification:

$$N_{2(tot)} = N_{2(ASW)} + N_{2(EA)} + N_{2(DEN)} \quad (1)$$

where $N_{2(ASW)}$ represents the air-saturated water concentration (ASW) due to the equilibration with the atmosphere at the atmospheric pressure and recharge water temperature, $N_{2(EA)}$ is the amount of N_2 due to excess air formation and $N_{2(DEN)}$ corresponds to N_2 stemming from complete denitrification (please see Text S2 and Fig. S1 for an explanation regarding the assumption of complete dentrification).

To obtain the noble gas recharge temperature (NGT), the amount of excess air (A) and the fractionation factor (F) necessary to accurately quantify excess air, we used the "closed-equilibrium" (CE) model (which assumes a concentration equilibrium between the entrapped air and water)[44,48,62] by applying an inverse modeling approach[45,63] employing the noble gas data (He, Ar and Kr) observed at each piezometer as input parameters (see Text S1). The CE-model is able to account for the continuous and progressive dissolution of entrapped air in porous media and thereby, provides an adequate estimate of excess air formation.[44,47]

$N_{2(ASW)}$ was calculated for the prevailing ambient pressure and estimated NGTs (Equation S1, Text S1) and $N_{2(EA)}$ was calculated according to the same parameters as well as A und F. Having calculated the atmospheric N_2 components ($N_{2(ASW)}$ and $N_{2(EA)}$), we can subsequently quantify the amount of N_2 produced by denitrification by solving for $N_{2(DEN)}$ (Equation 1).

Note that from here on we applied local polynomial regression fitting (i.e., "LOESS") to all data sets shown in Figures 3, 5, 6 to reduce noise and increase readability. LOESS uses a weighted, sliding-window to locally fit conditional means.[64] Please note that this approach smooths out the short-term variability of the data. However, without smoothing the data it would be inherently difficult to detect trends and pattern with the amount of data available. For a detailed discussion regarding issues during field work that let to data gaps, please see the supporting information (Text S2).

Results and Discussion

Spatial Variations of Hydraulic Conductivity and Total Cell Concentration

According to the results of the slug tests, hydraulic conductivity varies over two orders of magnitude within the approximately 40 m stream reach studied (Fig. 2a): P1 shows, with a mean of 15 (±4) m/d, the highest hydraulic conductivity, P5 ranks lowest, with 0.21 (±0.02) m/d, and P4 lies in between P1 and P5, with a mean k of 3.6 (±0.1) m/d.

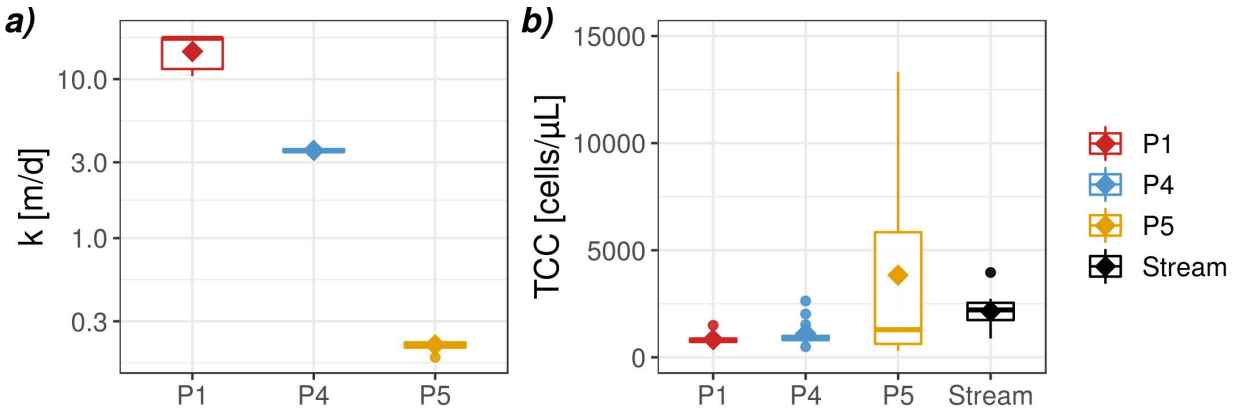

Figure 2: a) The hydraulic conductivity (log-scale) analyzed at P1 (n=5), P4 (n=13) and P5 (n=9); b) the total cell concentrations observed at P1, P4, P5 and at the stream (n=13 at each location); diamonds represent mean values.

The observed spatial differences in hydraulic conductivity seem to be reflected in the observed spatial differences of the total cell concentrations (Fig. 2): P1 shows the lowest mean concentration with 830 (±250), P4 exhibits a mean of 1100 (±600), and P5 shows the highest mean with 3800 (+/(−)4600) TCC (cells/μL) (please note that ± represents the standard deviation and that from here on +/(−) refers to standard deviations being larger than the mean concentrations).

In contrast to P1 and P4, P5 has a comparatively high variability in TCC. On average, the stream has higher TCC concentrations (2200±800 TCC cells/μL) than P1 and P4 but, interestingly, a lower mean than P5. The high variability in TCC at P5 also shows that

231 microbial activity can vary over several orders of magnitude within weeks, which most likely
232 also influences nitrate respiration rates.

233 TCC in all piezometers is unusually high for groundwater—the natural background con-
234 centration in groundwater with a residence time longer than a few days is $\sim$10 cells/μL.[65] The
235 high TCC concentrations observed in our samples demonstrate that stream water, which typ-
236 ically has higher TCC than groundwater, feeds the underlying groundwater and that travel
237 times from the stream to the groundwater must be short (i.e., a few days), as also indicated
238 by previous radon measurements.[54]

239 Moreover, our findings indicate that both parameters, k and TCC, are potentially linked:
240 a high hydraulic conductivity appears to correlate to low total cell concentrations (at P1)
241 and vice versa (at P5). These results are in line with previous studies,[23,59] which found that
242 microbial abundance greatly varies depending on the sediment texture because the sediment
243 texture governs the available surface area for microbial colonization and advective mass
244 transport of water, solutes and gases.

245 Key Parameters associated with Denitrification

246 Chemical species associated with denitrification show that the conditions in the riparian
247 groundwater of our study site are favorable for denitrification (Fig. 3; n=22 for each param-
248 eter and piezometer except for O_2): constantly high nitrate and DOC concentrations in the
249 river guarantee a permanent supply of two key chemical species for denitrification (Fig. 3a
250 and 3c, respectively). At the same time, the riparian groundwater is well below 10% of
251 oxygen saturation for most of the time of our experiment (Fig. 3b). Moreover, nitrate con-
252 centrations in all three piezometers are considerably reduced compared to the concentrations
253 in the stream, indicating denitrification (Fig. 3a).

254 P1 exhibits with 7% the highest mean O_2 saturation (i.e., O_2 in respect to $O_{2(ASW)}$),
255 P4 shows a slightly lower mean saturation with 6% and P5 has the lowest mean saturation
256 with 2% (Table 1). The locally observed oxygen concentrations seem to correspond to the

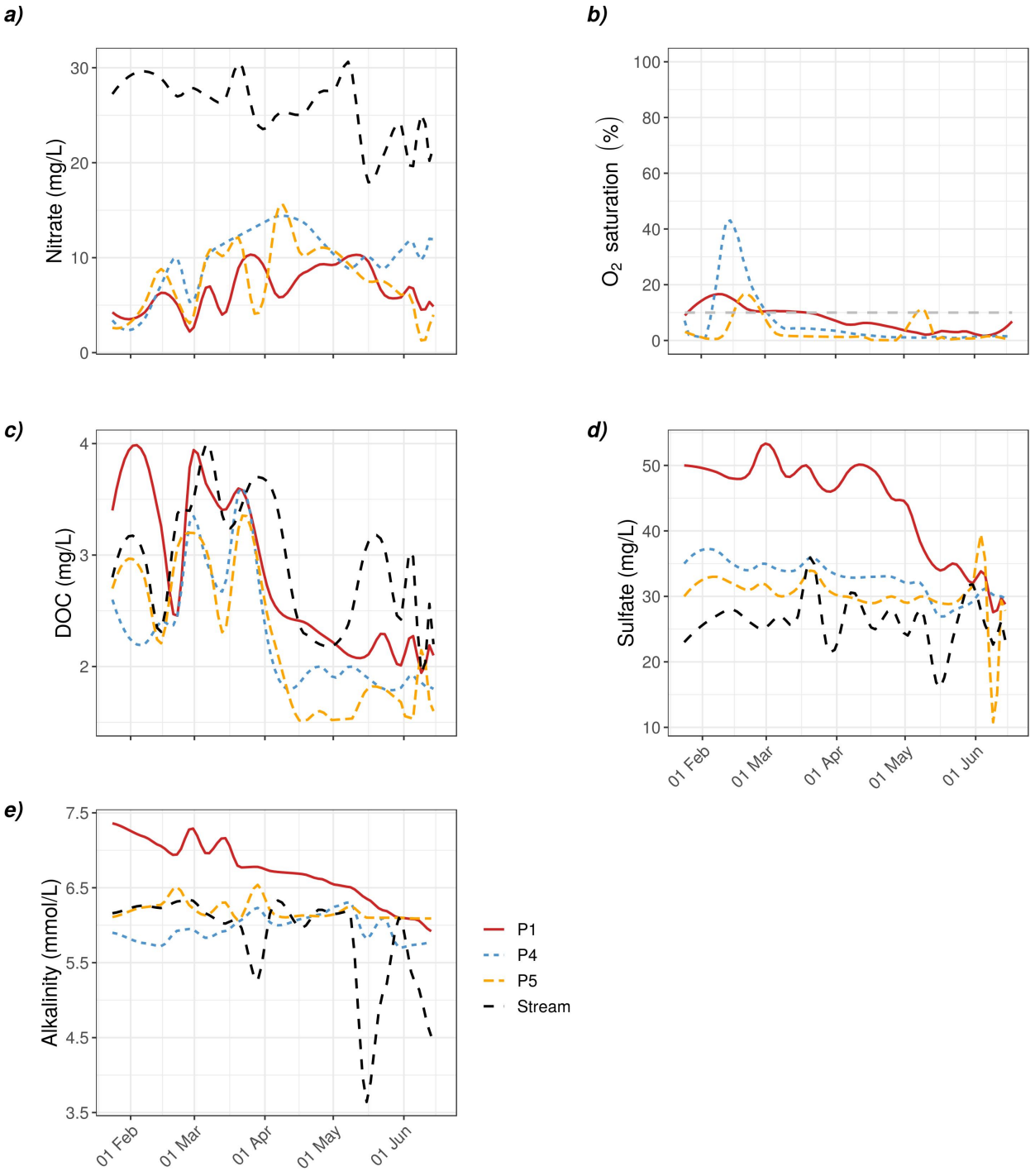

Figure 3: Concentrations of key parameters associated with denitrification (panels a–e). Gray dashed line in panel b shows 10% O_2 saturation indicating hypoxic conditions.

ambient hydraulic conductivity observed at the respective piezometer: the highest mean O_2 saturation found at P1 indicates that the highest k also results in the best hydraulic connection between the stream and the aquifer, delivering more oxygen rich stream water; whereas the lowest k at P5 leads to the lowest mean O_2 saturation.

The O_2 concentration time series of P4 and P5, however, sporadically show elevated levels, which most likely result from enhanced infiltration of oxygenated stream water to the riparian groundwater (Fig. 3b). These more aerobic conditions can inhibit denitrification—however, it has been shown that denitrification can still occur in anoxic microzones of bulk oxic sediments.[66]

Table 1: Number of total observations of N_2, O_2 and N_2 excess continuously analyzed at P1, P4, and P5, and their respective mean concentrations ± standard deviations. Number of observations differs between locations due to varying extents of data cleansing. [a] Refers to $N_{2(DEN)}$ + $N_{2(EA)}$ normalized to $N_{2(ASW)}$.

	P1	P4	P5
Number of total observations	4373	3977	2738
N_2 (10^{-5} cm^3_{STP}/g_{water})	156 (±10)	156 (±11)	161 (±13)
O_2 (10^{-5} cm^3_{STP}/g_{water})	5 (±4)	5 (±9)	2 (±3)
O_2 saturation (%)	7 (±5)	6 (+/(−)12)	2 (+/(−)5)
N_2 excess (%)[a]	18 (±4)	19 (±5)	23 (±5)
$N_{2(EA)}$ (10^{-5} cm^3_{STP}/g_{water})	60 (±40)	70 (±60)	80 (±60)

Also, sulfate and alkalinity concentrations are variable over time and again distinctively different in the three piezometers and the stream (Figs. 3d and e). For most of the time, we observed elevated concentrations of sulfate and alkalinity with respect to the stream water concentrations at all three piezometers, which is a clear indicator of denitrification occurring.

N_2 Production due to Denitrification

Previous studies used N_2/Ar to account and correct for N_2 injection due to excess air formation.[30–37,39,40,42] Thereby it is assumed that the produced excess air has an elemental composition matching that of free unfractionated air presuming the complete dissolution of air bubbles.[43,67] It has been shown, however, that unfractionated excess air has no mechanis-

tic physical basis as entrapped air bubbles almost never completely dissolve at groundwater recharge.[44,47,68] In contrast, the used CE-model approach to frame excess air formation is capable to correctly describe the partial dissolution of entrapped air in porous media. The conventional N_2/Ar approach would only be applicable if excess air was negligible ($A \sim 0$, $F \sim 0$; Fig. 4). At our study site most gas measurements, however, show considerable amounts of excess air being produced which is elementally strongly fractionated (Fig. 4). Thus, for the majority of the measurements only the CE-approach leads to a physically acceptable interpretation of excess air formation, which cannot be achieved by the N_2/Ar method.

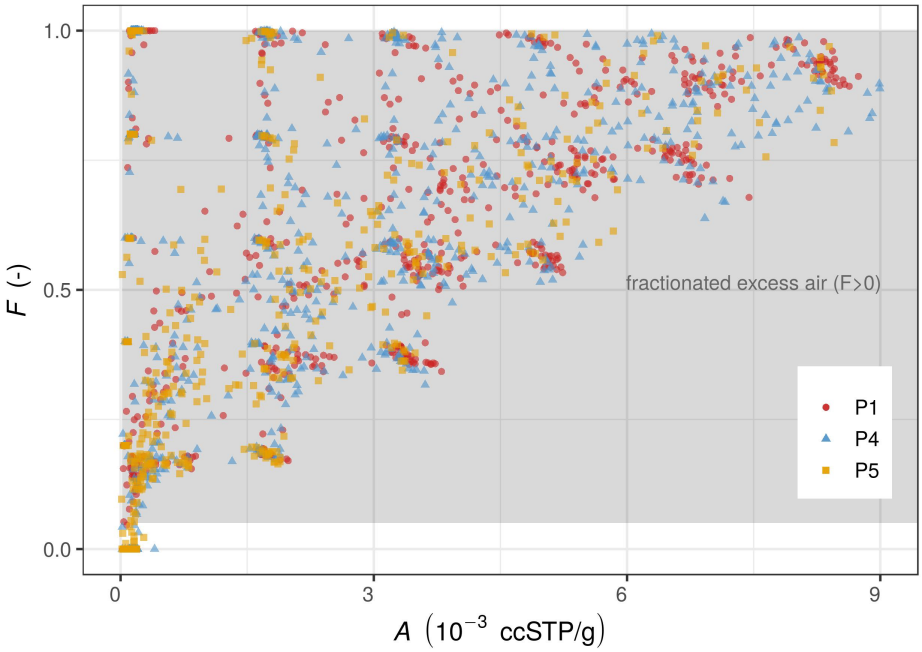

Figure 4: Amount of excess air (A) vs. elemental fractionation (F) calculated for the three piezometers using the CE-model. Grey area shows where excess air formation is affected by fractionation.

Figure 5 shows that $N_{2(tot)}$ concentrations vary spatially and temporally at all three piezometers and that they are distinctively elevated with respect to $N_{2(ASW)}$ concentrations. At P1, we observe the lowest mean concentration of $N_{2(EA)}$, whereas P5 exhibits on average about 30% more $N_{2(EA)}$ than P1 (Table 1, Fig. 5). Generally, $N_{2(EA)}$ decreases at all three piezometers towards the warmer summer months (see difference between black and grey data

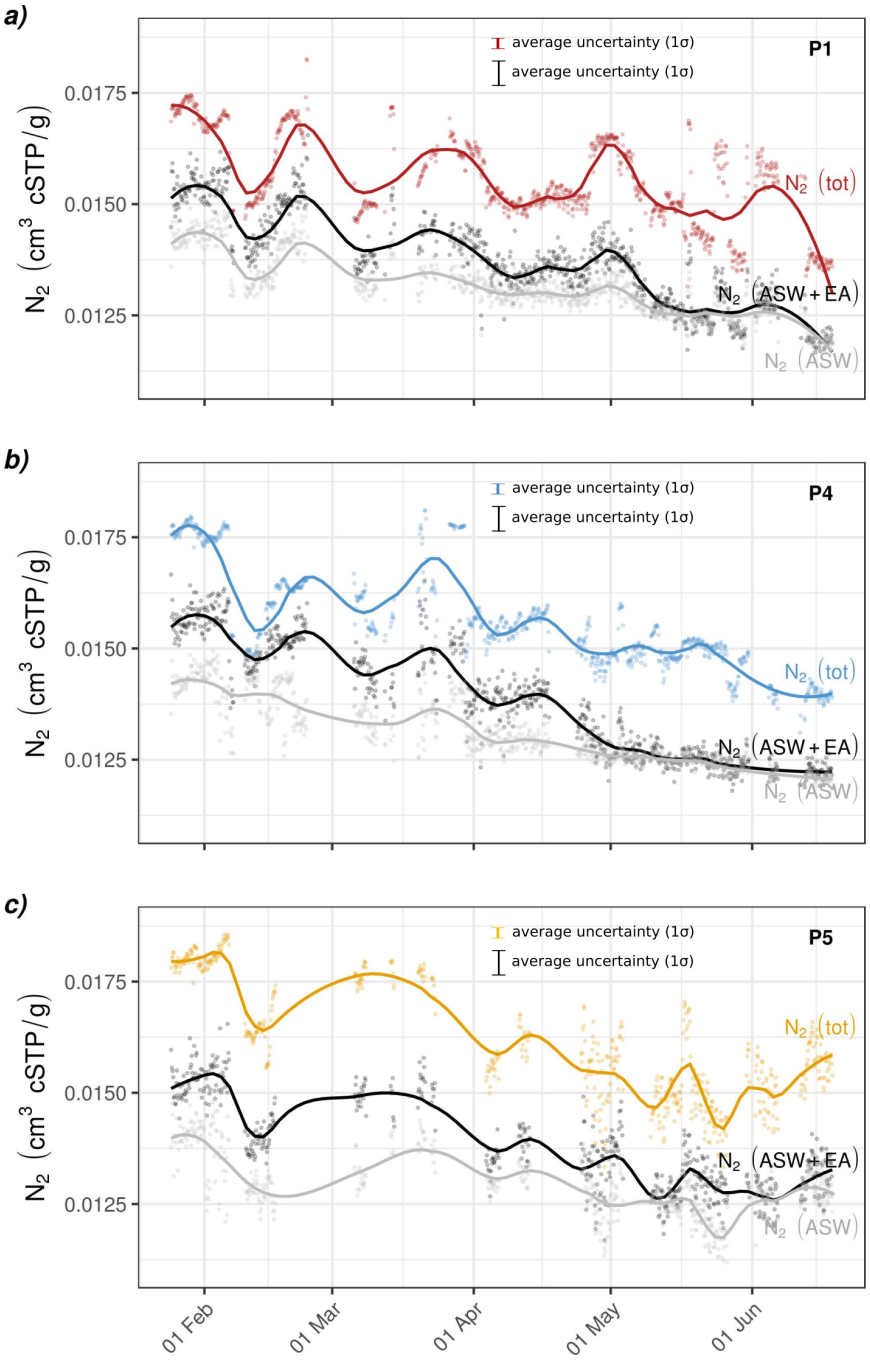

Figure 5: Colored lines (panel a in red=P1; panel b in blue=P4; panel c in orange=P5) show the observed $N_{2(tot)}$ concentrations; gray lines show the $N_{2(ASW)}$ concentrations for the respective piezometer; black lines show the sum of $N_{2(ASW)}$ and $N_{2(EA)}$; 1-σ indicates the averaged standard deviation of 5 aggregated data points. The difference between $N_{2(tot)}$ and $N_{2(ASW+EA)}$ represents the amount of N_2 originating from denitrification.

in Fig. 5). This might be related to increased clogging of the riverbed due to an enhanced biofilm growth, which in turn can reduce water infiltration.

$N_{2(EA)}$ concentrations vary to a great extent not only temporally but also spatially within this small scale of about 40 meters (Table 1). The lower hydraulic conductivities at P4 and P5 compared to P1 most likely explain the higher excess air content of P4 and P5 because air entrapment and immobilization of air bubbles strongly depend on the local sediment characteristics and are fostered in fine grained sediments.[46] Thus, we hypothesize that the different sediment textures observed at the three piezometers result in different feedback mechanisms between excess air formation, microbial growth and nutrient delivery, which in turn affect nitrate availability and turnover.

Figure 6 shows the prevailing hydraulic conditions (Panels a and b) during our experiment as well as the concentrations of NO_3^- (Panel c) that were estimated to have been denitrified for all three piezometers ($N_{2(DEN)}$, Equation 1). For the time of our experiment, an average concentration of 10 mg/L denitrified NO_3^- was present at P1 and P4, and 13 mg/L at P5. The average uncertainty to determine denitrification with the method presented is 2 mg/L NO_3^-. Interestingly, these mean values lie in a similar range at all three piezometers even though external conditions such as hydraulic conductivity and TCC concentrations are distinctively different at each piezometer. Since all piezometers, however, are constantly recharged by the same water source (i.e., receiving the same nitrate supply), this similarity can be explained reasonably well. Overall, the highest respiration of nitrate to N_2 observed at P5 can most likely be attributed to the overall lowest O_2 concentrations observed at this piezometer.

Denitrification, however, differs not only spatially but also temporally: from virtually no denitrification in February at P4 when O_2 levels at P4 were relatively high (Fig. 3b) to more than 22 mg/L of NO_3^- being respired in June at P1 when O_2 levels in P1 were lowest (Figs. 3b and 6). Figure 6 also demonstrates that the main difference in the concentration of denitrified NO_3^- between P5 and the other piezometers (i.e., P1 and P4) occurred in the colder months, when the latter had temporarily better but still low oxygenated conditions

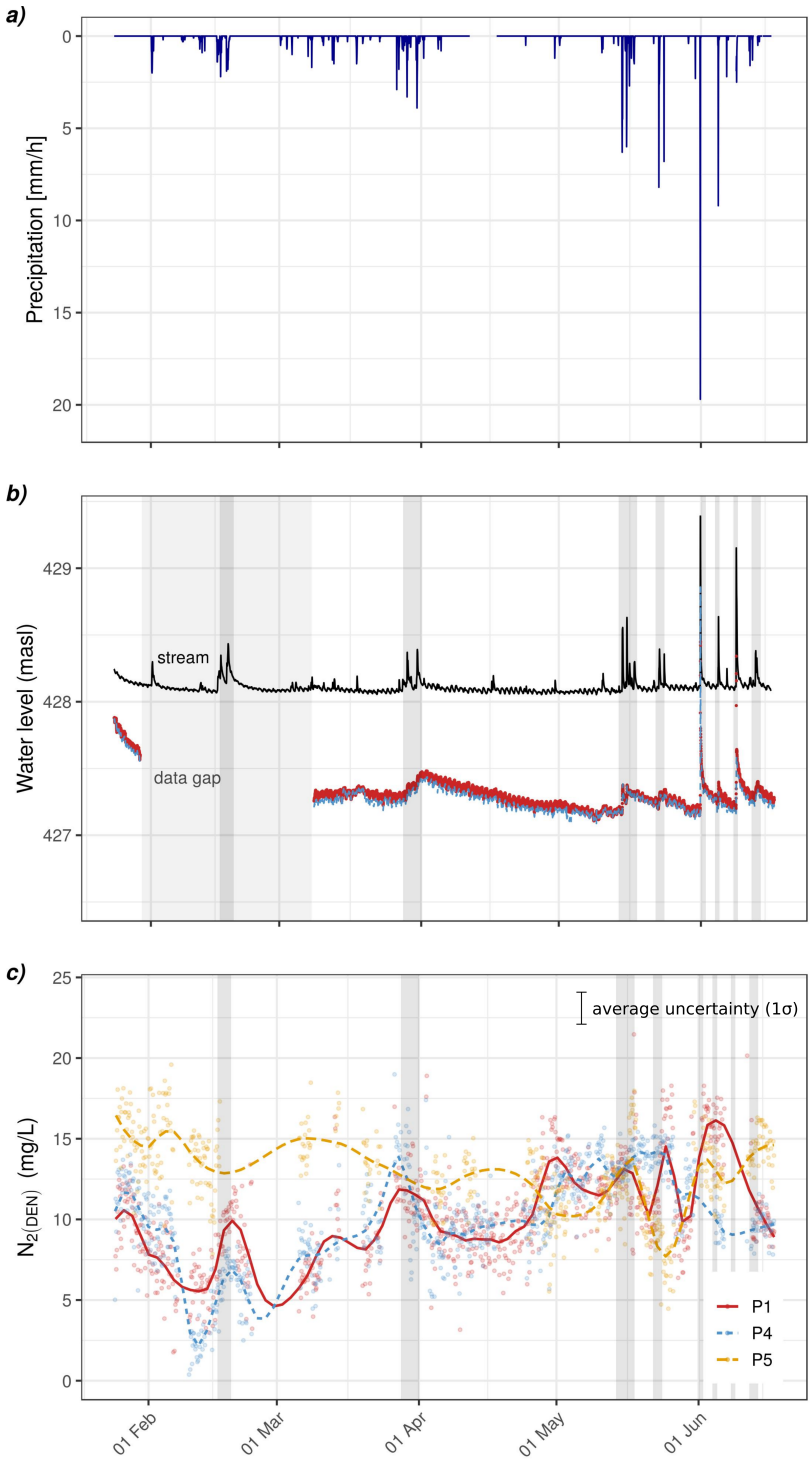

Figure 6: Panel a and b show the hydrological conditions for the duration of our experiment: precipitation observed at the study site and water levels of the Chriesbach (black) as well as P1 (red) and P4 (blue, dashed), respectively (data of P5 not available). Panel c illustrates estimated concentrations of N_2 originating from denitrification at P1, P4 and P5; error bar indicates averaged 1-σ uncertainty. Darker gray segments indicate high discharge events.

(Fig. 3b).

Moreover, piezometers P1 and P4 both show a response to higher discharge events (shown as darker gray segments in Fig. 6). Shortly after such events, denitrification in P1 and P4 seems to decrease, whereas P5 appears to remain rather unaffected. While this pattern can again be related to the different hydrogeologic properties, we would like to note that an in-depth interpretation of the relation between hydrological dynamics and denitrification is not possible without knowing the residence time and flow-paths of groundwater (see also Text S2).

The high temporal variability of denitrification most likely results from the dynamic interactions occurring in river-aquifer systems, where the infiltration of oxygenated river water (as sporadically observed at P4 and P5; Fig. 3b) reduces or inhibits denitrification. Moreover, the spatial differences in sediment characteristics and microbial activity (Fig. 2) are additional factors contributing to differences in space and time as these parameters influence flow paths and reaction rates.

P1 and P4 exhibit comparatively low $N_{2(DEN)}$ concentrations throughout January until mid March, whereas from end of March on, denitrification observed at P1 and P4 approximates that of P5. The overall increase in denitrification observed at P1 and P4 (Fig. 6) can be explained by the gradual decrease in O_2 saturation (Fig. 3b) and a potentially enhanced nitrate turnover due to higher microbial activities with increasing temperature.[11] The slight decrease in denitrification observed at P5 might result from an increased biofilm growth, which in turn can reduce the infiltration rate[69] and limit the delivery of nitrate-rich stream water to the riparian groundwater. An enhanced biofilm growth would limit infiltration rates at P5 to a greater extent than at P1 or P4 because of the already low hydraulic conductivity present at P5. The hypothesis of reduced infiltration rates as a consequence of partial clogging of the streambed in warmer summer months is further corroborated by the decline in DOC concentrations over time (Fig. 3c). The system studied is, however, apparently not DOC limited because denitrification still increases (P1 and P4) or stays the same (P5)

despite the decrease of DOC in the warmer summer months.

The highest observed value of respired nitrate (22 mg/L at P1) corresponds to ∼25% of dissolved N_2 originating from denitrification. This result aligns well with estimates of Wilson et al.,[32] who found that denitrification can account for up to 25% of N_2 in a limestone aquifer. Moreover, our results add experimental evidence to model-based findings[23] demonstrating the enormous capacity of riparian zones to convert nitrate to nitrogen gas and to also store this gas. Our experimental data also underscore previous other model-based findings[70] showing that respiration rates in riparian corridors can vary to great extents spatially and temporally and that losing streams can efficiently remove nitrate.[71]

We conclude that nitrate respiration to N_2 in riparian groundwater is highly variable in time and space, as denitrification is dependent on competing controls. On the one hand, a well connected stream-aquifer system fosters denitrification by constantly supplying enough nitrate and DOC. On the other hand, it can impede denitrification by also delivering O_2-rich stream water. A combination of a rapid low-cost method like the GE-MIMS combined with a physically meaningful excess air model presents a valuable new tool to study denitrification dynamics in fast-changing groundwater systems.

Acknowledgement

We thank four anonymous reviewers for their constructive feedback, which helped to improve this manuscript. We thank Benjamin Plüss, Wendelin Wild, Jonas Zbinden and Reto Britt for their support in setting up the field experiment. The AUA laboratory at Eawag is thanked for analyzing the water samples for nitrate, DOC, sulfate, alkalinity, nitrite and ammonium concentrations. Moreover, we thank Frederik Hammes and Michael Besmer for discussions about microbes in groundwater systems. Frederik Hammes is acknowledged for analyzing the TCC samples. The Federal Office for the Environment (FOEN) is thanked for providing the precipitation data. A.L.P. acknowledges funding by the EU Framework Programme for

Research and Innovation Horizon 2020 ITN "Hypotrain" (Grant: 641939) and Eawag.

Supporting Information Available

Supporting information (SI_Popp-et-al_ES&T.pdf) includes

- Text S1: Background information on dissolved (noble) gas theory;
- Text S2: Assumptions and limitations of this study;
- Text S3: Field work issues;
- Code S1: Noble gas data processing scripts;
- Figure S1: Nitrite and Ammonium data of P1, P4, P5 and the stream (weekly sampling);
- Figure S2: Stream water temperature and estimated NGTs for all piezometers;
- Figure S3: Picture of the study site including the stream, the piezometers and the location of the GE-MIMS;
- Table S1: Information about instruments used, limits of quantification and uncertainties for the data shown in Figure 3 (manuscript);
- Dataset S1: (Noble) gas data obtained at piezometer P1, P4 and P5;
- Dataset S2: CE-model results and subsequent calculations for piezometer P1, P4 and P5;
- Dataset S3: Data for Figure 3 (except for oxygen, which can be found in Dataset_S2), Figure 2 (microbial activity) and Figure S1 for all piezometers;
- Dataset S4: Hydraulic conductivity (k) data for all piezometers;

- Dataset S5: Stream water level data;
- Dataset S6: Groundwater level data of P4 and P5;
- Dataset S7: Precipitation and air temperature data recorded at station "Dübendorf-Empa".

This information is available free of charge via the Internet at `http://pubs.acs.org`.

References

(1) Rockström, J. et al. A safe operating space for humanity. *Nature* **2009**, *461*, 472–475.

(2) Mekonnen, M. M.; Hoekstra, A. Y. Global Gray Water Footprint and Water Pollution Levels Related to Anthropogenic Nitrogen Loads to Fresh Water. *Environ. Sci. Technol.* **2015**, *49*, 12860–12868.

(3) Stevens, C. J. Nitrogen in the environment. *Science* **2019**, *363*, 578–580.

(4) Sinha, E.; Michalak, A. M.; Balaji, V. Eutrophication will increase during the 21st century as a result of precipitation changes. *Science* **2017**, *357*, 405–408.

(5) WHO, Guidelines for Drinking-water Quality. *World Heal. Organ.* **2011**, *4*, 1–541.

(6) Yu, C. et al. Managing nitrogen to restore water quality in China. *Nature* **2019**, *567*, 516–520.

(7) EEC, Directive 91/676/EEC concerning the protection of waters against pollution caused by nitrates from agricultural sources. *Off. J. Eur. Communities* **1991**, *1*, OJ L 375, 31.12.1991, 1–8.

(8) UNEA, Towards a Pollution-Free Planet. 2017.

(9) Korom, S. F. Natural denitrification in the saturated zone: A review. *Water Resour. Res.* **1992**, *28*, 1657–1668.

(10) Davidson, E. A.; Seitzinger, S. The Enigma of Progress in Denitrification Research Denitrification. *Ecol. Appl.* **2006**, *16*, 2057–2063.

(11) Rivett, M. O.; Buss, S. R.; Morgan, P.; Smith, J. W. N.; Bemment, C. D. Nitrate attenuation in groundwater: a review of biogeochemical controlling processes. *Water Res.* **2008**, *42*, 4215–32.

(12) Groffman, P. M.; Butterbach-Bahl, K.; Fulweiler, R. W.; Gold, A. J.; Morse, J. L.; Stander, E. K.; Tague, C.; Tonitto, C.; Vidon, P. Challenges to incorporating spatially and temporally explicit phenomena (hotspots and hot moments) in denitrification models. *Biogeochemistry* **2009**, *93*, 49–77.

(13) Saunders, D. L.; Kalff, J. Denitrification Rates in the Sediments of Lake Memphremagog, Canada-USA. *Water Res.* **2001**, *35*, 1897–1904.

(14) Groffman, P. M.; Altabet, M. A.; Böhlke, J. K.; Butterbach-Bahl, K.; David, M. B.; Firestone, M. K.; Giblin, A. E.; Kana, T. M.; Nielsen, L. P.; Voyteck, M. A. Methods for measuring denitrification: diverse approaches to a difficult problem. *Ecol. Appl.* **2006**, *16*, 2091–2122.

(15) Smith, R. L.; Howes, B. L.; Duff, J. H. Denitrification in nitrate-contaminated groundwater: Occurrence in steep vertical geochemical gradients. *Geochim. Cosmochim. Acta* **1991**, *55*, 1815–1825.

(16) Peter, S.; Rechsteiner, R.; Lehmann, M. F.; Brankatschk, R.; Vogt, T.; Diem, S.; Wehrli, B.; Tockner, K.; Durisch-Kaiser, E. Nitrate removal in a restored riparian groundwater system: Functioning and importance of individual riparian zones. *Biogeosciences* **2012**, *9*, 4295–4307.

(17) Gu, C.; Anderson, W.; Maggi, F. Riparian biogeochemical hot moments induced by stream fluctuations. *Water Resour. Res.* **2012**, *48*, 1–17.

(18) Hill, A. R.; Devito, K. J.; Vidon, P. G. Long-term nitrate removal in a stream riparian zone. *Biogeochemistry* **2014**, *121*, 425–439.

(19) Ward, A. S.; Packman, A. I. Advancing our predictive understanding of river corridor exchange. *Wiley Interdiscip. Rev. Water* **2018**, *6*, e1327.

(20) Krause, S. et al. Ecohydrological interfaces as hot spots of ecosystem processes. *Water Resour. Res.* **2017**, *53*, 6359–6376.

(21) Packman, A. I.; Salehin, M. Relative roles of stream flow and sedimentary conditions in controlling hyporheic exchange. *Hydrobiologia* **2003**, *494*, 291–297.

(22) Mendoza-Lera, C.; Datry, T. Relating hydraulic conductivity and hyporheic zone biogeochemical processing to conserve and restore river ecosystem services. *Sci. Total Environ.* **2017**, *579*, 1815–1821.

(23) Newcomer, M. E.; Hubbard, S. S.; Fleckenstein, J. H.; Maier, U.; Schmidt, C.; Thullner, M.; Ulrich, C.; Flipo, N.; Rubin, Y. Influence of Hydrological Perturbations and Riverbed Sediment Characteristics on Hyporheic Zone Respiration of CO_2 and N_2. *J. Geophys. Res. Biogeosciences* **2018**, *123*, 902–922.

(24) Ranalli, A. J.; Macalady, D. L. The importance of the riparian zone and in-stream processes in nitrate attenuation in undisturbed and agricultural watersheds—A review of the scientific literature. *J. Hydrol.* **2010**, *389*, 406–415.

(25) Merill, L.; Tonjes, D. J. A review of the hyporheic zone, stream restoration, and means to enhance denitrification. *Crit. Rev. Environ. Sci. Technol.* **2014**, *44*, 2337–2379.

(26) Boyer, E. W.; Alexander, R. B.; Parton, W. J.; Li, C.; Butterbach-Bahl, K.; Donner, S. D.; Skaggs, R. W.; Grosso, S. J. D. Modeling denitrification in terrestrial and aquatic ecosystems at regional scales. *Ecological Applications* **2006**, *16*, 2123–2142.

(27) Kolbe, T.; de Dreuzy, J.-R.; Abbott, B. W.; Aquilina, L.; Babey, T.; Green, C. T.; Fleckenstein, J. H.; Labasque, T.; Laverman, A. M.; Marçais, J.; Peiffer, S.; Thomas, Z.; Pinay, G. Stratification of reactivity determines nitrate removal in groundwater. *Proc. Natl. Acad. Sci.* **2019**, *116 (7)*, 2494–2499.

(28) Ozima, M.; Podosek, F. *Noble Gas Geochemistry*; Cambridge University Press, 1984.

(29) Oana, S. Bestimmung von Argon in besonderem Hinblick auf gelöste Gase in natürlichen Gewässern. *J. Earth Sci. Nagoya Univ.* **1957**, *5*, 103–105.

(30) Kana, T. M.; Darkangelo, C.; Hunt, M. D.; Oldham, J. B.; Bennett, G. E.; Cornwell, J. C. Membrane Inlet Mass Spectrometer for Rapid High-Precision Determination of N_2, O_2, and Ar in Environmental Water Samples. *Anal. Chem.* **1994**, *66*, 4166–4170.

(31) Vogel, J. C.; Talma, A. S.; Heaton, T. H. Gaseous nitrogen as evidence for denitrification in groundwater. *J. Hydrol.* **1981**, *50*, 191–200.

(32) Wilson, G. B.; Andrews, J. N.; Bath, A. H. Dissolved gas evidence for denitrification in the Lincolnshire Limestone groundwaters, eastern England. *J. Hydrol.* **1990**, *113*, 51–60.

(33) Blicher-Mathiesen, G.; McCarty, G. W.; Nielsen, L. P. Denitrification and degassing in groundwater estimated from dissolved dinitrogen and argon. *J. Hydrol.* **1998**, *208*, 16–24.

(34) Green, C. T.; Puckett, L. J.; Böhlke, J. K.; Bekins, B. A.; Phillips, S. P.; Kauffman, L. J.; Denver, J. M.; Johnson, H. M. Limited Occurrence of Denitrification in Four Shallow Aquifers in Agricultural Areas of the United States. *J. Environ. Qual.* **2008**, *37*, 994.

(35) Weymann, D.; Well, R.; Flessa, H.; Heide, C. V. D.; Deurer, M.; Meyer, K.; Konrad, C.; Walther, W.; Drive, T.; North, P.; Zealand, N. Groundwater N_2O emission

factors of nitrate-contaminated aquifers as derived from denitrification progress and N_2O accumulation. *Biogeosciences* **2008**, *5*, 1215–1226.

(36) Böhlke, J. K.; Antweiler, R. C.; Harvey, J. W.; Laursen, A. E.; Smith, L. K.; Smith, R. L.; Voytek, M. A. Multi-scale measurements and modeling of denitrification in streams with varying flow and nitrate concentration in the upper Mississippi River basin, USA. *Biogeochemistry* **2009**, *93*, 117–141.

(37) Kennedy, C. D.; Genereux, D. P.; Corbett, D. R.; Mitasova, H. Relationships among groundwater age, denitrification, and the coupled groundwater and nitrogen fluxes through a streambed. *Water Resour. Res.* **2009**, *45*, 1–15.

(38) Izbicki, J. A.; Teague, N. F.; Hatzinger, P. B.; Böhlke, J. K.; Sturchio, N. C. Groundwater movement, recharge, and perchlorate occurrence in a faulted alluvial aquifer in California (USA). *Hydrogeol. J.* **2015**, *23*, 467–491.

(39) McAleer, E. B.; Coxon, C. E.; Richards, K. G.; Jahangir, M. M.; Grant, J.; Mellander, P. E. Groundwater nitrate reduction versus dissolved gas production: A tale of two catchments. *Sci. Total Environ.* **2017**, *586*, 372–389.

(40) Szymczycha, B.; Kroeger, K. D.; Crusius, J.; Bratton, J. F. Depth of the vadose zone controls aquifer biogeochemical conditions and extent of anthropogenic nitrogen removal. *Water Res.* **2017**, *123*, 794–801.

(41) Stenger, R.; Clague, J. C.; Morgenstern, U.; Clough, T. J. Vertical stratification of redox conditions, denitrification and recharge in shallow groundwater on a volcanic hillslope containing relict organic matter. *Sci. Total Environ.* **2018**, *639*, 1205–1219.

(42) Eschenbach, W.; Budziak, D.; Elbracht, J.; Höper, H.; Krienen, L.; Kunkel, R.; Meyer, K.; Well, R.; Wendland, F. Possibilities and limitations of validating modelled nitrate inputs into groundwater at the macroscale using the N2/Ar-method. *Grundwasser* **2018**, *23*, 125–139.

(43) Kipfer, R.; Aeschbach-Hertig, W.; Peeters, F.; Stute, M. Noble Gases in Lakes and Ground Waters. *Rev. Miner. Geochemistry* **2002**, *47*, 615–700.

(44) Klump, S.; Cirpka, O. A.; Surbeck, H.; Kipfer, R. Experimental and numerical studies on excess-air formation in quasi-saturated porous media. *Water Resour. Res.* **2008**, *44*, 1–15.

(45) Aeschbach-Hertig, W.; Peeters, F.; Beyerle, U.; Kipfer, R. Interpretation of dissolved atmospheric noble gases in natural waters. *Water Resour. Res.* **1999**, *35*, 2779–2792.

(46) Klump, S.; Tomonaga, Y.; Kienzler, P.; Kinzelbach, W.; Baumann, T.; Imboden, D. M.; Kipfer, R. Field experiments yield new insights into gas exchange and excess air formation in natural porous media. *Geochim. Cosmochim. Acta* **2007**, *71*, 1385–1397.

(47) Holocher, J.; Peeters, F.; Aeschbach-Hertig, W.; Kinzelbach, W.; Kipfer, R. Kinetic model of gas bubble dissolution in groundwater and its implications for the dissolved gas composition. *Environ. Sci. Technol.* **2003**, *37*, 1337–1343.

(48) Aeschbach-Hertig, W.; El-Gamal, H.; Wieser, M.; Palcsu, L. Modeling excess air and degassing in groundwater by equilibrium partitioning with a gas phase. *Water Resour. Res.* **2008**, *44*, 1–12.

(49) Mächler, L.; Peter, S.; Brennwald, M. S.; Kipfer, R. Excess air formation as a mechanism for delivering oxygen to groundwater. *Water Resour. Res.* **2013**, *49*, 6847–6856.

(50) Mächler, L.; Brennwald, M. S.; Kipfer, R. Argon concentration time-series as a tool to study gas dynamics in the hyporheic zone. *Environ. Sci. Technol.* **2013**, *47*, 7060–7066.

(51) Brennwald, M. S.; Schmidt, M.; Oser, J.; Kipfer, R. A portable and autonomous mass spectrometric system for on-site environmental gas analysis. *Environ. Sci. Technol.* **2016**, *50*, 13455–13463.

(52) Uyanik, S.; Demirel, S.; Dursun, N.; Kilic, A.; Cinar, O.; Sahinkaya, E. Simultaneous heterotrophic and sulfur-oxidizing autotrophic denitrification process for drinking water treatment: Control of sulfate production. *Water Res.* **2011**, *45*, 6661–6667.

(53) Hayakawa, A.; Hatakeyama, M.; Asano, R.; Ishikawa, Y.; Hidaka, S. Nitrate reduction coupled with pyrite oxidation in the surface sediments of a sulfide-rich ecosystem. *J. Geophys. Res. Biogeosciences* **2013**, *118*, 639–649.

(54) Kurth, A.-M.; Weber, C.; Schirmer, M. How effective is river restoration in re-establishing groundwater-surface water interactions?—A case study. *Hydrol. Earth Syst. Sci.* **2015**, *19*, 2663–2672.

(55) AWEL, Stelle 177 : Chriesbach vor Glatt. 2018; `https://www.hw.zh.ch/chemie/fg/177_L.pdf`.

(56) AWEL, Zürcher Gewässer 2012 Ausblick, Entwicklung Zustand. 2012; `https://awel.zh.ch/internet/baudirektion/awel/de/wasser/gewaesserschutz/wasserqualitaet/{\_}jcr{\_}content/contentPar/downloadlist{\_}0/downloaditems/1315{\_}1540908017631.spooler.download.1429193158805.pdf/AWEL{\_}Gewaesserbericht{\_}2012{\_}Flyer{\_}A4.pdf`.

(57) Bear, J. *Dynamics of Fluids in Porous Media*; Dover publications, Inc.: New York, 1972; pp 1–764.

(58) Bouwer, H.; Rice, R. C. A slug test for determining hydraulic conductivity of unconfined aquifers with completely or partially penetrating wells. *Water Resour. Res.* **1976**, *12*, 423–428.

(59) Mendoza-Lera, C.; Frossard, A.; Knie, M.; Federlein, L. L.; Gessner, M. O.; Mutz, M. Importance of advective mass transfer and sediment surface area for streambed microbial communities. *Freshw. Biol.* **2016**, *62*, 133–145.

(60) Prest, E.; Hammes, F.; Kötzsch, S.; van Loosdrecht, M.; Vrouwenvelder, J. Monitoring microbiological changes in drinking water systems using a fast and reproducible flow cytometric method. *Water Res.* **2013**, *47*, 7131–7142.

(61) 3M Liqui-Cel, A high level of consistency and control. 2017; `http://multimedia.3m.com/mws/media/1412485O/3m-liqui-cel-membrane-contactors-liquid-degasgaslc-1096-pdf`.

(62) Aeschbach-Hertig, W.; Peeters, F.; Beyerle, U.; Kipfer, R. Palaeotemperature reconstruction from noble gases in ground water taking into account equilibration with entrapped air. *Nature* **2000**, *405*, 1040–1044.

(63) Ballentine, C.; Hall, C. Determining paleotemperature and other variables by using an error-weighted, nonlinear inversion of noble gas concentrations in water. *Geochim. Cosmochim. Acta* **1999**, *63*, 2315–2336.

(64) Jacoby, W. G. Loess: a nonparametric, graphical tool for depicting relationships between variables. *Elect. Stud.* **2000**, *19*, 577–613.

(65) Besmer, M. D.; Epting, J.; Page, R. M.; Sigrist, J. A.; Huggenberger, P.; Hammes, F. Online flow cytometry reveals microbial dynamics influenced by concurrent natural and operational events in groundwater used for drinking water treatment. *Sci. Rep.* **2016**, *6*, 1–10.

(66) Briggs, M. A.; Day-Lewis, F. D.; Zarnetske, J. P.; Harvey, J. W. A physical explanation for the development of redox microzones in hyporheic flow. *Geophys. Res. Lett.* **2015**, *42*, 4402–4410.

(67) Heaton, T. H. E.; Vogel, J. C. "Excess air" in groundwater. *J. Hydrol.* **1981**, *50*, 201–216.

575 (68) Stute, M.; Schlosser, P.; Clark, J. F.; Broecker, W. S. Paleotemperatures in the South-
576 western United States Derived from Noble Gases in Ground Water. *Science* **1992**, *256*,
577 1000–1003.

578 (69) Battin, T. J.; Sengschmitt, D. Linking Sediment Biofilms, Hydrodynamics, and River
579 Bed Clogging: Evidence from a Large River. *Microb. Ecol.* **1999**, *37*, 185–196.

580 (70) Dwivedi, D.; Arora, B.; Steefel, C. I.; Dafflon, B.; Versteeg, R. Hot Spots and Hot
581 Moments of Nitrogen in a Riparian Corridor. *Water Resour. Res.* **2018**, *54*, 205–222.

582 (71) Shuai, P.; Cardenas, M. B.; Knappett, P. S.; Bennett, P. C.; Neilson, B. T. Denitrifi-
583 cation in the banks of fluctuating rivers: The effects of river stage amplitude, sediment
584 hydraulic conductivity and dispersivity, and ambient groundwater flow. *Water Resour.*
585 *Res.* **2017**, *53*, 7951–7967.

Graphical TOC Entry